Journal of Constructional Steel Research 139 (2017) 397–410

Contents lists available at ScienceDirect

Journal of Constructional Steel Research

Numerical assessment of slab-interaction effects on the behaviour of steel-concrete composite joints

Claudio Amadio, Chiara Bedon *, Marco Fasan

University of Trieste, Department of Engineering and Architecture, Piazzale Europa 1, 34127 Trieste, Italy

ARTICLE INFO

Article history:
Received 18 April 2017
Received in revised form 14 August 2017
Accepted 4 October 2017
Available online xxxx

Keywords:
Steel-concrete composite joints
Finite element numerical modelling
Experimental validation
Seismic performance
Isolated slab
Resisting mechanisms
Design

ABSTRACT

In current design practice for seismic resistant steel braced frames, general rules and standard provisions are aimed to ensure a structural behaviour for beam-to-column joints of non-braced spans as close as possible to perfect hinges. This is done to prevent any kind of interaction with the bracing systems, in particular under horizontal loads. However, the global performance of composite joints is markedly affected by the structural interaction between the concrete slab and the steel components and - especially during seismic events - struts can occur in the slab at the beam-to-column intersection.

In this paper, the possibility of realizing a composite joint that behaves as moment-resisting under gravitational loads and essentially as hinged under horizontal loads is investigated. Aiming to assess the actual slab-interaction effects on the overall response, a full 3D Finite Element (FE) model representative of a beam-to-column composite joint taking part of a braced frame is described in ABAQUS and validated towards past full-scale experiments. A parametric study is hence proposed, by accounting for three geometrical configurations, being characterized by (i) isolated slab with absence of rebar continuity (i.e. fully disconnected slab and steel joint only), (ii) presence of slab with partial column interaction (i.e. isolated slab and continuity of rebar), (iii) presence of fully interacting slab. It is shown that, if properly detailed, a joint with isolated slab and continuous rebars can be used in non-braced spans of composite braced frames without affecting the behaviour of the bracing system (i.e. as in presence of a hinge). Nonetheless, the composite beam can be designed as continuous on multiple supports under vertical loads, hence leading to a reduction of the steel cross-sectional size.

1. Introduction

The seismic behaviour of steel-concrete composite joints is highly affected by the structural interaction occurring between the concrete slab and the steel components at the beam-to-column intersection. This aspect has specific relevance for the design of braced frames, where the overall performance of the joints placed in non-braced spans should be as close as possible to perfect hinges, hence preventing any kind of interaction with the bracing systems [1,2]. During a seismic event, compression forces can typically arise in the concrete slab in the vicinity of the column, leading to the occurrence of struts in contact with the steel flanges. In this regard, it is thus necessary to fully understand the influence of possible interaction effects among the joint components, in order to properly assess their global response.

To this aim, the structural behaviour of composite joints attracted a multitude of research studies, over the past decades, see for example [3–16]. Most of past experimental and numerical outcomes currently represent the reference background for design procedures in use for steel-concrete composite structures. In [8–9], careful consideration was given to the detection of concrete confinement effects in composite columns, including an assessment of strength and stiffness degradation phenomena.

Several experimental tests have been carried out on various joint typologies, aiming to explore their stiffness, strength, ductility and energy dissipation capacity.

Finite-Element (FE) numerical models developed to further investigate past experimental tests have been also proposed during last years, aiming to predict the inelastic response of exterior and interior beam-to-column joints, both under monotonic or cyclic loads (see for example [17–20]). Despite the large number of research contributions, however, most of the past FE investigations have been mainly focused on the prediction of the global behaviour only of various joint typologies.

In [20], differing from existing research projects, a full 3D refined FE numerical study was proposed, aiming to assess both the global and local behaviour of steel-concrete composite joints. Taking advantage of accurate FE numerical models developed in the ABAQUS computer software [21] and validated towards full-scale experimental test results available in the literature for a welded composite joint, it was shown that the actual geometrical and mechanical properties of a given joint and its components details, as well as their reciprocal interactions, can be properly taken into account, hence resulting in rather accurate

* Corresponding author.
E-mail address: chiara.bedon@dia.units.it (C. Bedon).

https://doi.org/10.1016/j.jcsr.2017.10.003
0143-974X/

simulation of even complex mechanical phenomena. Critical discussion of FE results suggested in fact the use of refined FE predictions as a valid support and/or alternative to costly and time consuming full-scale experimental tests, since allowing extensive parametric investigations of composite joints - including a wide set of geometrical and mechanical configurations for steel-concrete structural systems - with careful consideration for both global and local effects.

2. Objectives

In this paper, following [21], a further Finite Element (FE) numerical investigation is proposed for beam-to-column steel-concrete composite joints. As a reference joint typology, the full-scale experimental study reported in [23] is taken into account and explored. At a preliminary stage of the ongoing research study, the experimental specimen presented in [23] is first numerically reproduced (see Section 3), so to validate all the mechanical and geometrical assumptions for the reference FE model. The so implemented model is then used to numerically assess and emphasize the actual effects of slab-to-column interactions on the overall performance of the examined steel-concrete composite joint, when subjected to various loading conditions. To avoid the interaction between the slab and the column, the Eurocode 8 [2] suggests in fact a 'total disconnection' of the slab components near the column. In this paper, conversely, the possibility to take advantage of the continuity of the longitudinal rebar is investigated.

In particular, through a set of parametric FE analyses, three different geometrical configurations are considered for the reference full-scale specimen, being aimed to characterize the actual load bearing performance of (i) the steel joint alone (i.e. isolated slab with absence of rebar continuity), (ii) the isolated slab with continuity of longitudinal rebar, and (iii) an almost fully interacting slab (even with a small gap, on one side of the column only).

Based on the FE comparative results partly summarized in this paper, it is shown that the isolation of the slab is typically associated to important effects on the structural performance of the joint. As far as the slab is properly isolated from the column - even with a small gap - any kind of over-strengthening effect on the given joint response is in fact fully avoided, hence allowing to better control the overall seismic response of the braced frame it belongs. In particular, under the action of lateral loads (e.g. earthquakes or wind), as also in line with current design regulations [1,2], the joint can be described as perfectly hinged, and the lateral loads are directly transferred to the bracing system (even in presence of continuous longitudinal rebar). Under the action of gravitational loads, in contrary, the continuity of the longitudinal rebar is typically associated to a mostly clamped performance of the joint, hence with an overall response of the steel-concrete composite beams which is close to continuity on multiple supports.

3. Finite element numerical investigation

3.1. Reference experimental specimen and past test results

As a reference geometrical configuration, the steel-concrete composite joint experimentally investigated in [23] was taken into account, see Fig. 1. The reference specimen, based on [23], consisted of Italian IPE300 type steel beams, with 2.1 m the nominal length, and an HEB260 type column, with 2.77 m the total height. The steel beams were used to support a concrete slab, 120 mm in thickness and 1 m in width (see also the transversal cross-section given in Fig. 2). In it, the longitudinal rebar was given by 8ϕ14 and 8ϕ6 bars, lying on the top and bottom slab layers respectively. Steel shear studs, 19 mm in diameter and 75 mm in total height, were then used to provide a fully rigid mechanical connection between the slab and the steel beams. Those shear connectors were 75 mm and 150 mm spaced along the transversal and longitudinal beams axis, respectively.

In terms of slab-to-column connection, at the time of past experimental tests, a 25 mm wide gap was realized on the left side of the specimen, being representative of the key aspect for the full assembly procedure and investigation, see Fig. 2(b). Such a design choice was in fact aimed to explore the occurrence and propagation of specific failure mechanisms in the specimen, due to slab-to-column mechanical interactions. Four M20 bolts (8.8 their resistant class) were finally used to

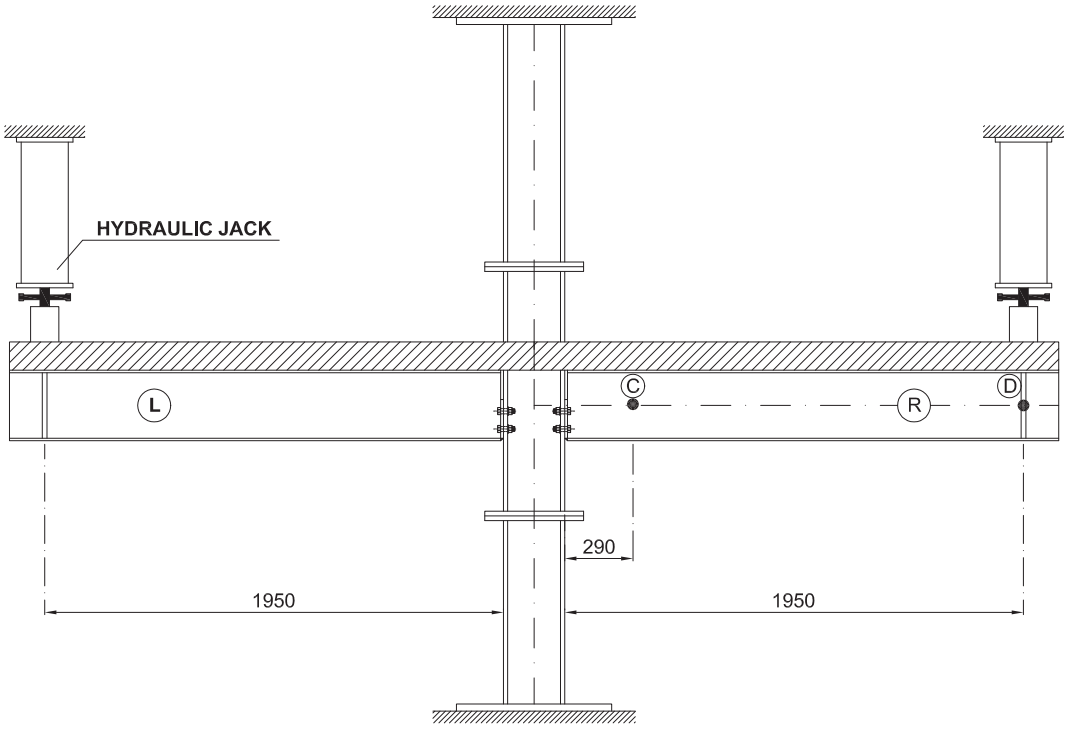

Fig. 1. Reference full-scale specimen object of investigation, in accordance with [23]. Front view (nominal dimensions given in mm).

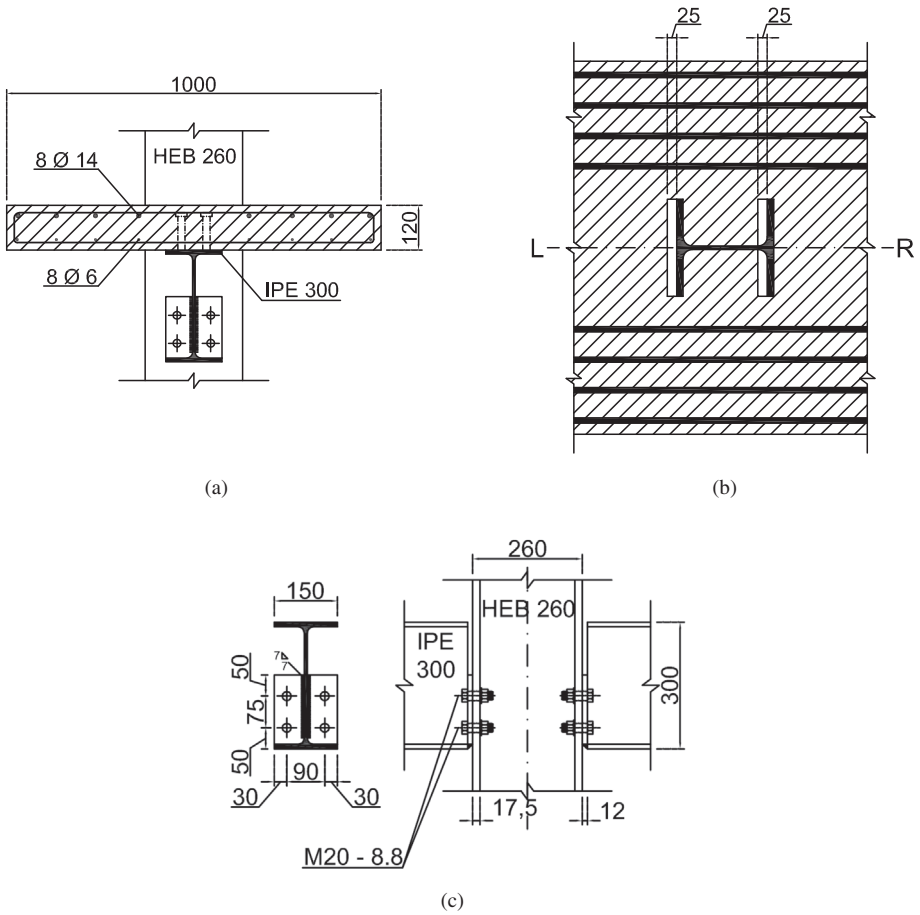

Fig. 2. Geometrical details for the reference full-scale specimen, in accordance with [23]. Transversal cross-section, (b) slab-to-column detail (top view, with $a = 25$ mm the gap size), (c) bolted joint (lateral and front views). Nominal dimensions given in mm.

assembly the steel joint, see Fig. 2(c). Further details on test methods and geometrical or mechanical features of the full-scale specimen are reported in [23].

In accordance with Fig. 3, three different loading configurations were then considered during the past experimental investigation. Due to the presence of unsymmetrical gaps in the slab, the examined loading conditions were detected to reproduce hogging moment on both the sides of the slab (see Fig. 3(a) and (b)), as well as the effects deriving from gravitational loads. (Fig. 3(c)). In doing so, monotonic loads were applied on the column slab via two hydraulic jacks at the beams ends, with 1950 mm their distance from the column flanges. The corresponding vertical deflections were continuously monitored, at a distance of 290 mm from the column flanges (see 'point C' in Fig. 1).

3.2. FE modelling approach and solving method

A full 3D refined modelling approach was developed in the ABAQUS computer software [22], aiming to preliminary reproduce the actual geometrical and mechanical properties of the reference specimen recalled in Section 3.1. The earlier FE approach proposed in [21] was taken into account and further extended, so that the accuracy of numerical predictions could be guaranteed, both in terms of global and local observations and findings.

The reference FE numerical model ('M0', in the following) was hence described by taking into account the nominal geometrical features of the experimental specimen derived from [23]. In doing so, the presence of possible imperfections in steel members (i.e. out-of-square of flanges) was preliminary neglected, based also on lack

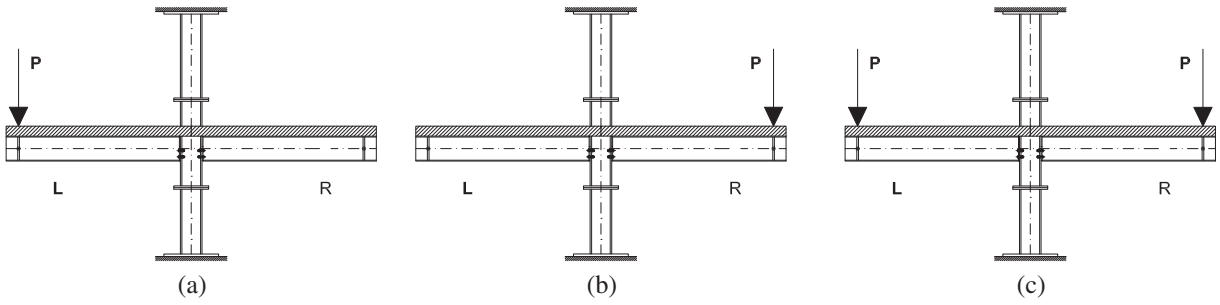

Fig. 3. Loading configurations for the reference full-scale specimen, in accordance with [23]. (a) Hogging moment L, (b) hogging moment R, and (c) gravitational loads (front view).

of detailed experimental measurements. For the M20 steel bolts, in addition, their resisting cross-section was described in the form of an effective circular section, with $A_{eff} / A_{nom} = 0.78$ the effective-to-nominal section ratio.

Careful consideration was paid for the geometrical and mechanical characterization of the single joint components (i.e. steel beams, bolts and shear studs, column, plus the concrete slab and the steel rebars), as well as for their reciprocal interactions (see Sections 3.2.1 and 3.2.2). Monotonic loading conditions according to Fig. 3 were then carried out in the form of Dynamic/Explicit analyses, with quasi-static application of loads.

After validation of FE assumptions for the reference M0 model, see Section 3.2.3, the M0 assembly was further explored, by taking into account additional FE configurations, being representative of different loading conditions as well as several typologies of slab-to-column mechanical interactions of technical interest for design purposes.

3.2.1. Model assembly

The full M0 model consisted of solid brick elements for all the steel components and the concrete slab (C3D8R type elements). C3D8R solid elements were used also for the joint detailing, based on available technical drawings for the experimental specimen, so to ensure reliable FE estimations in terms of slab-to-column interactions. Beam elements (B31 type of ABAQUS library) were indeed used for the steel rebars only, see Fig. 4.

For brick elements, the adopted mesh pattern consisted in a regular scheme of 8-node solid elements, with reference edge size comprised between 8 mm and 60 mm. Based also on preliminary sensitivity studies, mesh refinement was adopted especially in the vicinity of geometrical irregularities, discontinuities and joint details only, to ensure the accuracy of results through the full simulations. A coarse mesh pattern was indeed preferred for the model regions not directly involved in mechanical interactions, to preserve a certain computational efficiency of FE models. The typical FE assembly consisted in fact in a total number of 23,000 solid elements and 1300 beam elements, corresponding to 120,000 DOFs.

Following [21] as well as in accordance with recent example of refined FE modelling for composite structures (see for example [24]), a key role was assigned to contact mechanical interactions, being aimed to reproduce all the possible contacts at the steel-to-steel or steel-to-concrete interfaces. The shear stud connectors were fully embedded within the concrete slab mesh, via the *embedded* constraint of ABAQUS, so to reproduce a fully rigid connection between steel connectors and the surrounding concrete. The same *embedded* constraint was also used for the steel rebars, as conventionally in use for steel-concrete composite beams and structural systems (i.e. [21,24–30].

A fully rigid connection, being represented by the *tie* constraint was also used as general interaction law between all the welded steel components, hence possible relative displacements and rotations, as well as progressive damage phenomena in the vicinity of the welded connections, were fully neglected.

Finally, major effects were assigned to *surface-to-surface* contact interactions. In doing so, a set of multiple combinations of *normal* and *tangential* contact options was defined, being representative of mechanical interactions at the steel-concrete or steel-steel interfaces of structural components. Different input features for these mechanical contacts were assigned at the interface between (a) the steel beams (top flange) and the supported concrete slab; (b) the concrete slab and the steel column flanges/web; (c) the steel beams and the column flanges. As a general rule, the *hard contact* definition was used to characterize the *normal* behaviour of two instances in contact. As such, possible separation between the involved surfaces was allowed in presence of tensile pressures, while full transmission of compressive stresses among theme was guaranteed (without compenetration of instances) also in the damaged phase. Variations in the earlier defined surface-to-surface contact interactions were given by input data for their *tangential* behaviour (*penalty* approach) and specifically by the reference values for the adopted static friction coefficients μ. Frictionless sliding mechanisms ($\mu = 0$) were in fact accounted at the interface between each steel bolt and the surrounding holes edges of joint/column flanges, while a conventional value $\mu = 0.5$ was used for all the other steel-concrete contact surfaces.

3.2.2. Materials

Experimental tests carried out on small samples and reported in [23] were taken into account, for the mechanical characterization of materials constitutive laws. In the case of all the steel members and components, in particular, a set of Von Mises elasto-plastic stress-strain laws was defined, while the *concrete damaged plasticity* ('CDP', in the following) damage model was used for the concrete slab. Experimental mechanical properties provided in [23] were considered for all the steel components (see Table 1), with $E_s = 200$GPa, $\nu_s = 0.3$ and $\rho_s = 7850$ Kg/m^3.

Nominal stress and strain values were taken into account in the case of bolts - due to lack of experimental tests on single components - according to their actual resistance class. The same approach was considered for the shear studs, as also in accordance with [21].

In terms of CDP input parameters, the mechanical calibration of both tensile and compressive constitutive behaviour was carried out in accordance with [21,31,32], as well as on the base of the experimental results derived from the small concrete specimens reported in [23]. Despite the limits of the continuous damage CDP formulation for predicting detailed cracking and local phenomena, as well as damage propagation in concrete under impact (i.e. [33,34].), past applications to steel-concrete composite systems or concrete structural components in general, including other brittle constructional materials like masonry and glass, proved the reliability of qualitative CDP quasi-static estimations (see for example [35–41]).

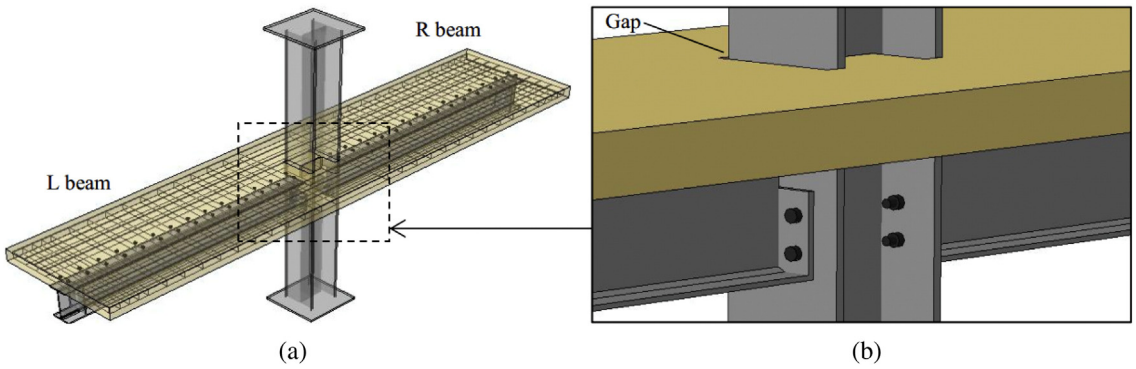

Fig. 4. Finite Element numerical model ('M0') representative of the reference experimental specimen, in accordance with [23]. (a) Axonometry and (b) joint detail, with mesh hidden from view (ABAQUS).

Table 1
Mechanical properties for steel members, in accordance with [21,23].

	Yielding stress $f_{y,s}$ [N/mm^2]	Ultimate stress $f_{u,s}$ [N/mm^2]	Ultimate strain $\varepsilon_{u,s}$ [%]
Beams	316	429	32.6
Column	338	485	30.6
Φ6 bars	387	537	28.7
Φ14 bars	421	668	26.2
Bolts[a]	640	800	30
Shear studs[a]	430	430	30

[a] Nominal mechanical properties.

Assuming a nominal ultimate strain for concrete equal to $\varepsilon_c = 0.0035$ [32], in particular, the compressive stress-strain constitutive law for the CDP formulation takes the form:

$$\frac{\sigma_c}{f_{cm}} = \frac{k\eta - \eta^2}{1 + (k-2)\times\eta} \tag{1}$$

where the compressive stress σ_c in concrete at a given strain level ε_c is given by the ratio:

$$\eta = \frac{\varepsilon_c}{\varepsilon_{c1}} \tag{2}$$

with

$$\varepsilon_{c1} = 0.7 f_{cm}^{0.31} \le 2.8 \tag{3}$$

In Eq. (3), ε_{c1} is representative of the compressive strain in concrete at the peak compressive stress, while

$$k = \frac{01.05 E_{cm} \times \varepsilon_{c1}}{f_{cm}} \tag{4}$$

for Eq. (1), with $f_{cm} = 27$ MPa and $E_{cm} = 30{,}000$ MPa [23].

In order to account for crushing and tensile cracking of concrete, the non-dimensional stiffness degradation parameter d_c (being equal to 1 for fully cracked concrete and 0 for uncracked concrete, respectively), representative of crushing damage in the slab, was then also defined as [32]:

$$d_c = 1 - \frac{\sigma_c / E_{c0}}{\varepsilon_c^{pl} + \sigma_c / E_{c0}}, \tag{5}$$

with $E_{c0} = E_{cm}$ the initial elastic modulus derived from the experimental tests and ε_c^{pl} the equivalent plastic strain, being defined as a function of the inelastic strain ε_c^{in}:

$$\varepsilon_c^{pl} = b_c \times \varepsilon_c^{in} = b_c \times (\varepsilon_c - \sigma_c / E_{c0}), \tag{6}$$

while $0 \le b_c = 0.7 \le 1$ is a compressive coefficient derived from [33].

In terms of tensile behaviour of concrete in cracked phase, a similar approach was followed. The stress-strain constitutive law, in this case, was defined as [32,42,43]:

$$\frac{\sigma_t}{f_t} = f(w) - \frac{w}{w_c} f(w_c) \tag{7}$$

with

$$f(w_c) = \left[1 + \left(\frac{c_1 w}{w_c}\right)^3\right] \exp\left(-\frac{c_2 w}{w_c}\right), \tag{8}$$

where w represents the crack opening displacement, while

$$w_c = 5.14 \frac{G_f}{f_{ct}} \tag{9}$$

is the crack opening displacement at which stress can no longer be transferred.

In Eq. (8), moreover, $c_1 = 3$ and $c_2 = 6.93$ are two material constants (values in use for Normal Weight Concrete), while f_{ct} in Eq. (9) can be calculated as [32]:

$$f_{ct} = 0.7 \times \left(0.3 f_{ck}^{2/3}\right) = 0.7 \times \left(0.3 \times (f_{cm} - 8)^{2/3}\right) \tag{10}$$

In Eq. (9), finally, the fracture energy of concrete was estimated as (see for example [44]):

$$G_f \approx \frac{G_F}{2.5} \tag{11}$$

with $G_F = 0.15$ N/mm the reference fracture energy value, as estimated on the base of the average size of aggregates for the examined experimental specimen.

3.2.3. Investigated geometrical configurations

Aiming to numerically assess the effects of slab-to-column interactions on the actual overall performance of the selected composite specimen, as well as on the occurrence and propagation of failure mechanisms in the so assembled steel-concrete components, three further FE models were derived from the M0 case:

(i) 'M0-steel' = fully isolated slab, including gaps on all the possible surfaces of interaction with the column, with absence of rebar continuity (i.e. fully disconnected slab and steel joint only, see Fig. 5(a)). In this model both the concrete slab and the steel rebars were deprived of continuity;
(ii) 'M0-iso' = presence of slab with partial column interaction (i.e. isolated slab and continuity of rebar, see Fig. 5(b));
(iii) 'M0-full' = presence of fully interacting slab and rebars' continuity.

It is worth noting that models 'M0-steel' and 'M0-full' represent limit conditions that are usually dealt with in the structural analysis practice as hinged or fixed supports, respectively.

For these three models, mechanical and geometrical features were kept equal to the reference M0 assembly, with major variations given by geometrical detailing and reciprocal contact interactions for the concrete slab and the steel rebars. In terms of solving approach, monotonic, quasi-static simulations were carried out in the form of Dynamic/Explicit analyses, by taking into account all the loading scenarios schematized in Fig. 3. As a further reference loading condition of practical interest for design of composite joints, the scenario given in Fig. 5(c) was also explored, being of particular interest for seismic design purposes.

4. Validation and discussion of FE numerical results

The 'M0' model described in Section 3 was first assessed and validated towards the corresponding experimental test results, by taking into account the reference loading configurations proposed in Fig. 3.

For sake of brevity, a brief overview and discussion is proposed in the following Sections, including the antisymmetric loading condition depicted in Fig. 5(c). All the collected load-displacement curves are intended as representative of displacements measured on the R beam control point (see 'point C' in Fig. 1).

Taking advantage of the refined FE modelling approach proposed in this research contribution, further comparative results are then critically presented for the investigated models, giving evidence of major effects due to slab-to-column interactions (see also Section 5).

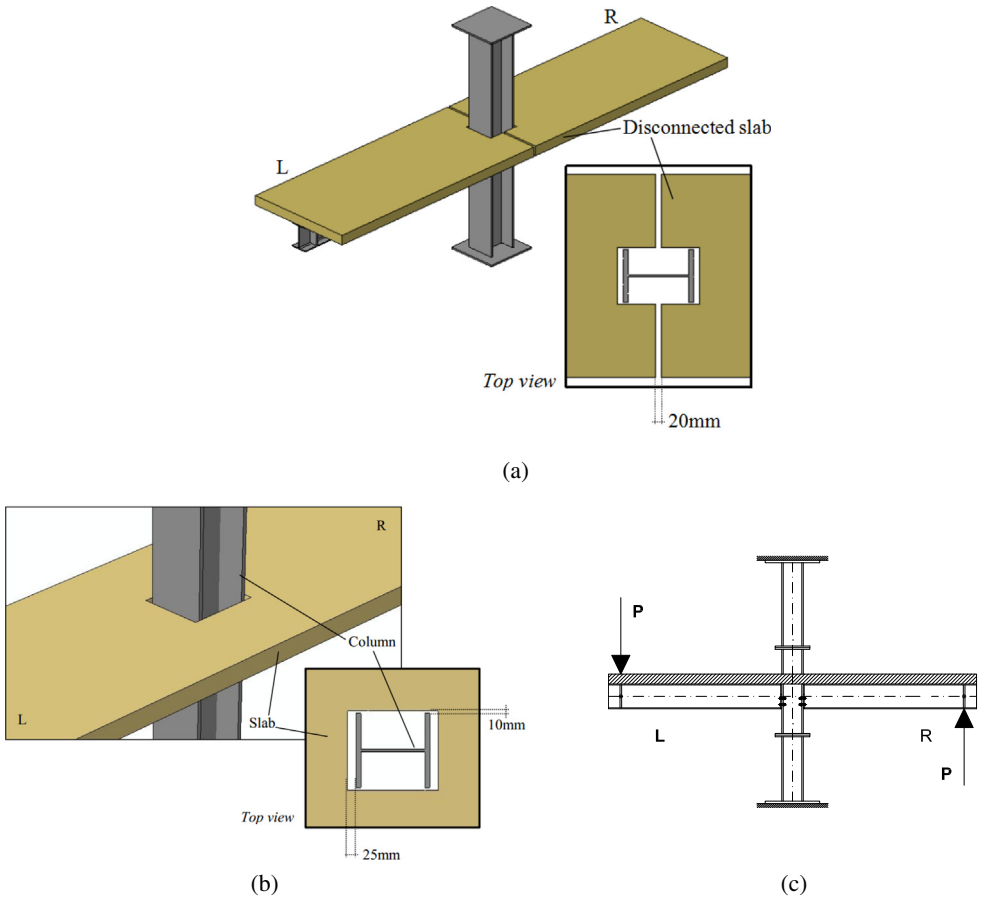

Fig. 5. Overview of FE numerical models included in the parametric study. (a) Fully isolated slab with rebar discontinuity ('M0-steel', detail) and (b) fully isolated slab with rebar continuity ('M0-iso'), axonometries from ABAQUS, with (c) antisymmetric loading condition.

4.1. Hogging moment

The reference 'M0' numerical model, as well as the FE models mentioned in Section 3.2.3, were first analysed under the L and R hogging moment configurations given in Fig. 3(a) and (b) respectively. In Fig. 6, evidence is given to both the 'hogging L' (slab in contact) and 'hogging R' (isolated slab) performances of the full-scale specimen, together with the corresponding 'M0' estimations.

As shown, as also in accordance with the earlier validation of the same full 3D FE numerical approach reported in [21] for another steel-concrete composite joint typology, a rather close correlation was generally observed between the actual M0 predictions and the past experimental measurements, hence suggesting further extension of the current FE study for investigating the effect of slab-to-column interactions.

Basically, the overall performance of the 'M0' specimen under the assigned loading configurations resulted characterized by three separate phases, see Fig. 6. Close agreement can be observed in terms of uncracked initial stiffness of the joint, as well as ultimate resistance, lying in the range of ≈110 kN. At this stage, partial overestimation of

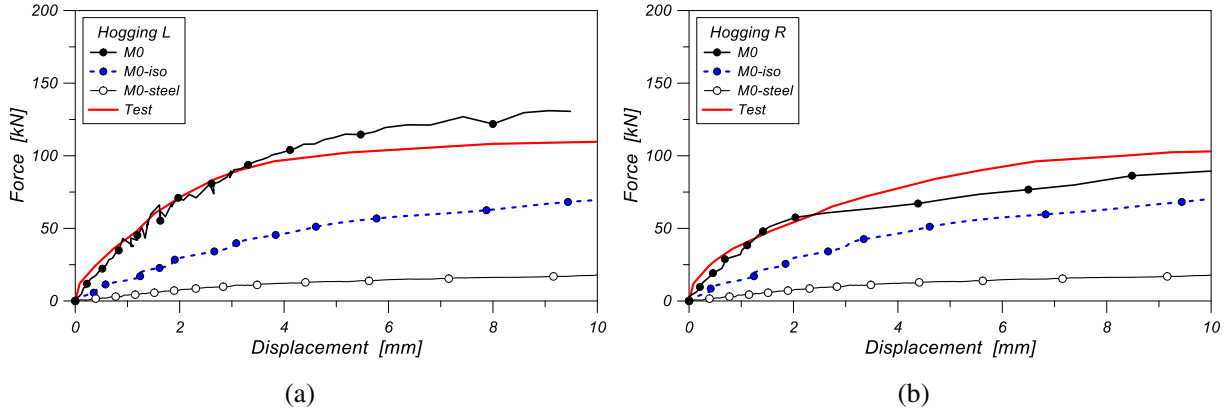

Fig. 6. FE load-displacement results, as obtained for the reference full-scale specimen and for the examined FE models under (a) 'hogging L' or (b) 'hogging R' loading conditions (ABAQUS).

the ultimate resistance of the specimen can be noticed, up to 10–15% the experimental value. In addition, see Fig. 6(a) and (b), it is possible to observe that for the 'M0' model, limited variations were achieved in terms of overall stiffness and resistance of the joint, hence signifying a rather negligible effect due to the presence of the unsymmetrical gap. In fact, a steel-concrete composite joint reacts, at the beam-to-column intersections, with the occurrence of different strut-and-tie mechanisms. Following the Eurocode 8 Annex C [1], three resisting mechanisms may occur in a composite joint, depending on the nodal configuration: (i) 'mechanism 1' – direct compression on the column flange, (ii) 'mechanism 2' – compressed concrete struts inclined to the column sides, and (iii) 'mechanism 3' – direct compression on the studs of the transversal beam. Thus, for the tested specimen, the gap realized in the slab prevents the occurrence of 'mechanism 1' but cannot avoid 'mechanism 2'. The almost comparable resistance between the left and right sides of the node may therefore derive from yielding of the longitudinal rebars which anticipate crashing of the concrete slab region in compression (due the activation of the 'mechanism 2'). However, a similar behaviour (with lower resistance) can be observed for the 'M0-iso' model, where all the interactions between the column and the slab are avoided. This behaviour is counter-intuitive and suggests the activation of other resistant mechanisms with respect to those defined by the Eurocode 8 for steel-concrete composite joints. The latter aspect is further investigated in Section 5.

Actually, see Fig. 7, plastic regions first occur and propagate in the steel column and joint flanges of the 'M0' configuration as far as measured displacements at the control point lie in the range of 1.5–2 mm.

Both Φ6 and Φ14 longitudinal rebars also first start to yield at a displacement of the R beam of ≈1.5 mm, with tensile cracking of the concrete slab and partial crushing on the R side, where direct contact exists with the column flange. As a result, as far as plastic regions further propagate in the column web and in the beam, see Fig. 7(c) and (d), both the rebars and the concrete slab are not able to provide further resisting contribution to the joint, with progressive propagation of damage in all the specimen components (see for example Fig. 8). Following Fig. 7 and the design criteria recently proposed in [45] for seismic resistant steel joints, performance levels for steel-concrete composite joints could be also univocally detected.

Worth of interest, in Fig. 6, is the overall performance of the 'M0-iso' model, where the lack of full interaction between the concrete slab and the column web still provides stiffness and resistance performances for the joint which lie in the same order of magnitude of the 'M0' specimen. As a result, compared to the 'M0-steel' configuration, typically characterized by limited stiffness and resistance and modelled in structural analysis as pinned connection, the 'M0-iso' configuration proved to have an overall structural behaviour in close correlation with that of the 'M0' system, for the examined joint under hogging L and R moments. In this sense, due to the absence of

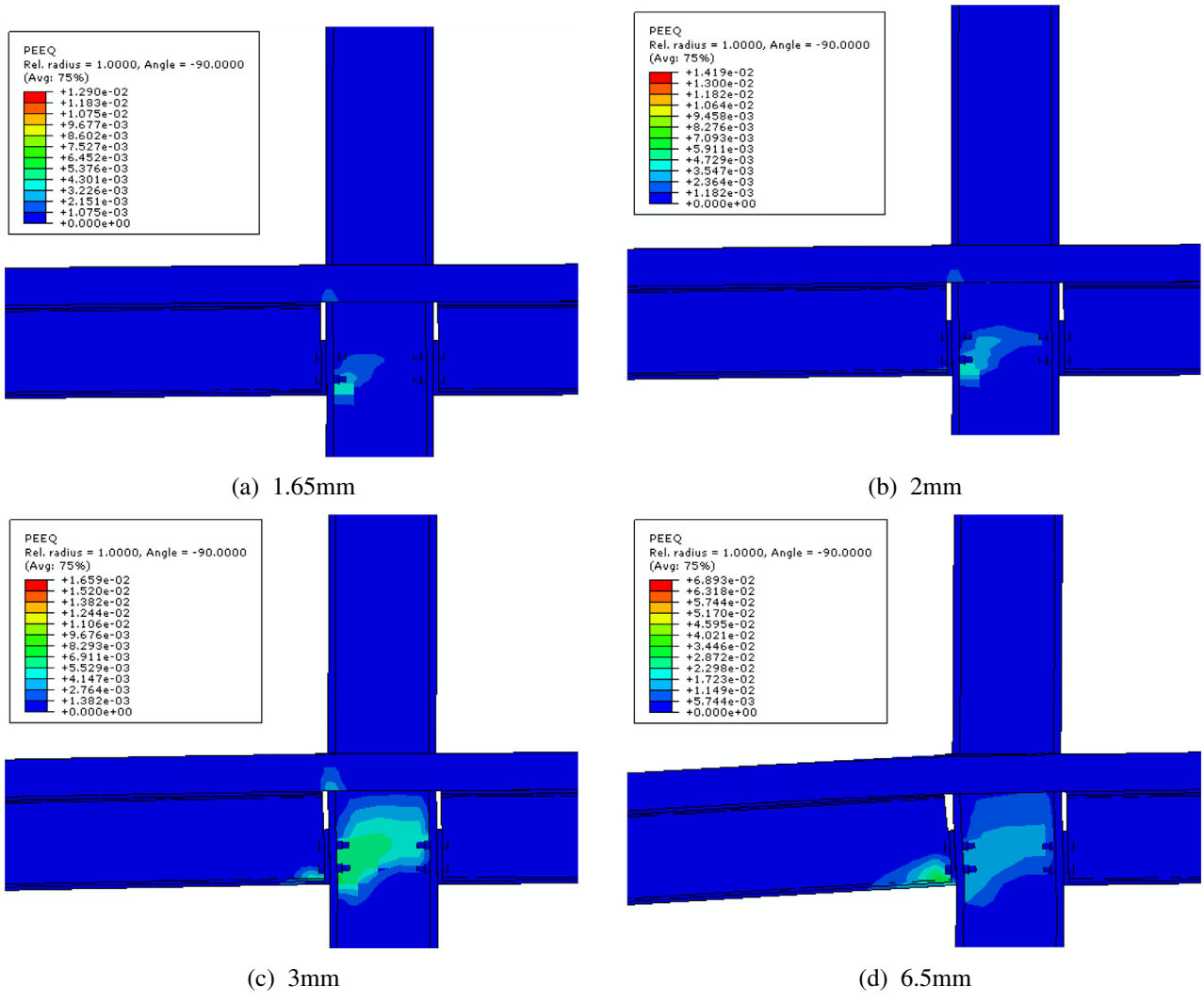

Fig. 7. FE results for the M0 model under 'hogging L' loading condition (ABAQUS), with evidence propagation of plastic regions as a function of the measured control point deflection.

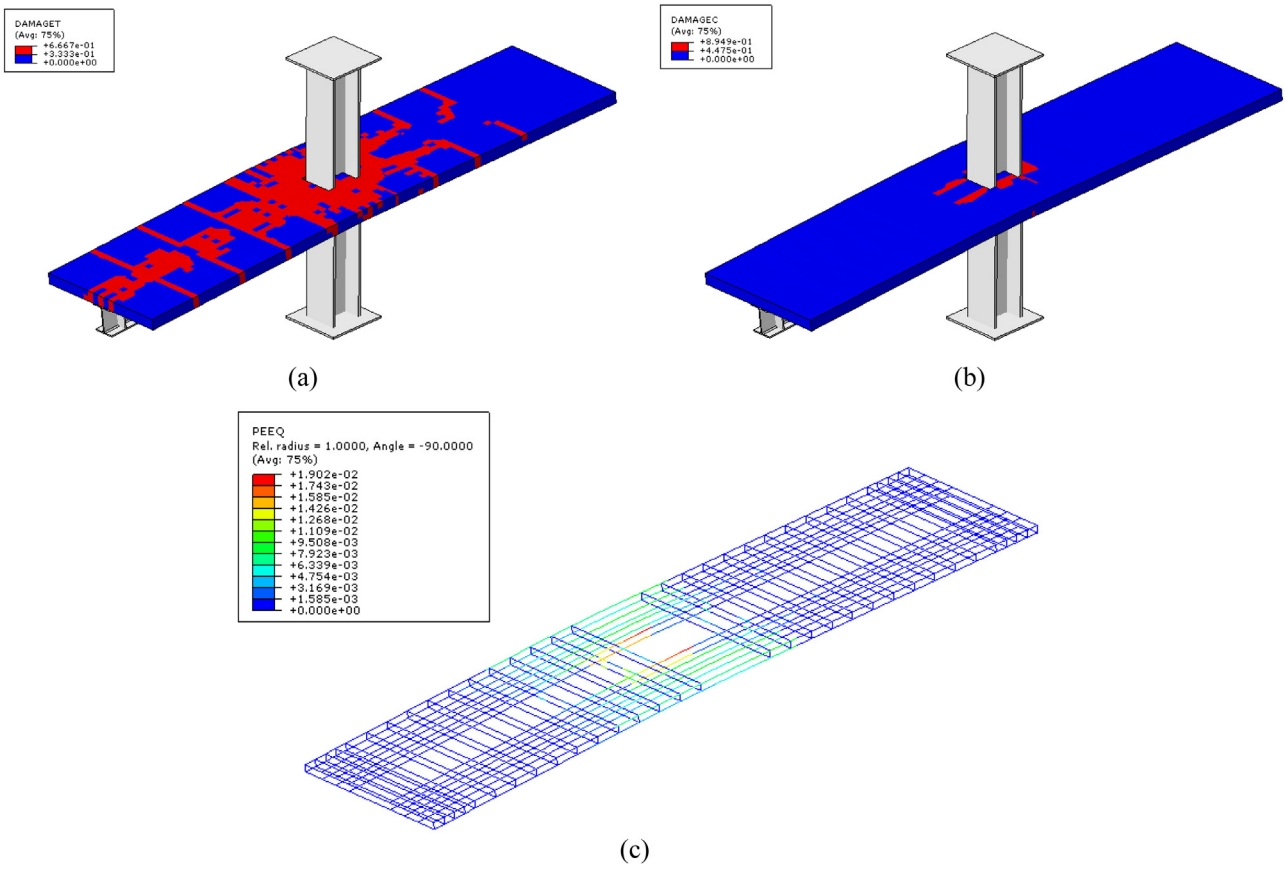

Fig. 8. FE observation of (a) tensile cracking and (b) crushing in the concrete slab (key: blue = uncracked, red = cracked), with (c) evidence of yielding in the steel rebars, as obtained for the M0 model under the 'hogging L' condition, at a measured deflection of 6.5 mm (ABAQUS). (For interpretation of the references to color in this figure legend, the reader is referred to the web version of this article.)

contact interactions at the slab-to-column surfaces for the M0-iso model, further explorations were undertaken (see Section 5), aiming to justify the increase in stiffness and resistance compared to the steel joint only.

4.2. Gravitational loads

The same FE model assemblies were then analysed under gravitational loads, see Fig. 3(c).

Compared to Section 4.1, partial correlation in the observed overall performances was typically captured by the examined models, as also expected. Also in the latter case, see Fig. 9, the FE modelling approach proved to offer accurate estimations, compared to the reference experimental specimen.

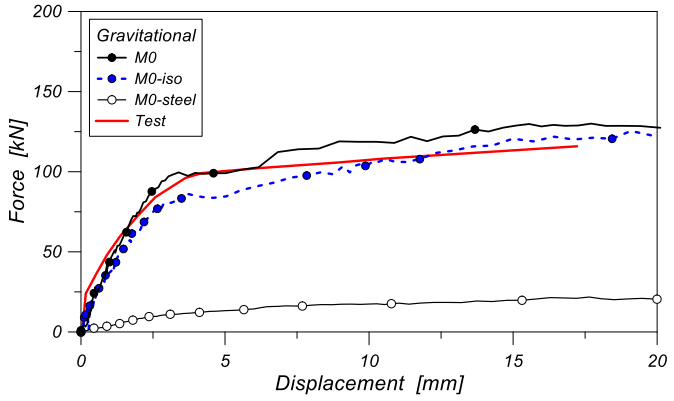

Fig. 9. FE load-displacement results, as obtained for the reference full-scale specimen and for the examined FE models under the 'gravitational' loading condition (ABAQUS).

In terms of overall performance of the joint under gravitational loads, in particular, a critical comparative observation of FE results was carried out, so that major effects deriving from the concrete slab configurations could be properly exploited. Basically, as also partly highlighted in Section 4.1, the resisting mechanisms typically depends in fact on three aspects, being represented by (i) compressive resistance of the column web, (ii) propagation of tensile and compressive in the joint flange and (iii) amount of maximum stresses taken up by longitudinal rebars in the slab.

For the specific loading condition, being associated to simultaneous application of hogging moments for both the L and R beams, a marked increase of the overall resistance was observed in terms of load-displacement relationships proposed in Fig. 9, as compared with Fig. 6. This effect was found to mainly derive from lack of premature crushing of concrete. In fact, under the examined loading condition, the hogging moment is the same on both the sides of the column, leading to a uniform tensile tension in the longitudinal rebars, thus avoiding the activation of resisting mechanisms in the slab.

The overall resistance of the joint, when subjected to gravitational loads, is mostly dependent on the compressive resistance of the column web, the joint flanges and the longitudinal rebars in the slab. As such, despite the lack of mechanical interaction between the slab and the column, the 'M0-iso' model proved to offer an overall resistance and stiffness in the same range of magnitude of the 'M0' specimen, see Fig. 9.

In Fig. 10, in this regard, the distribution of stresses (plastic region plus vectorial representation) is also proposed for the same 'M0-iso' model

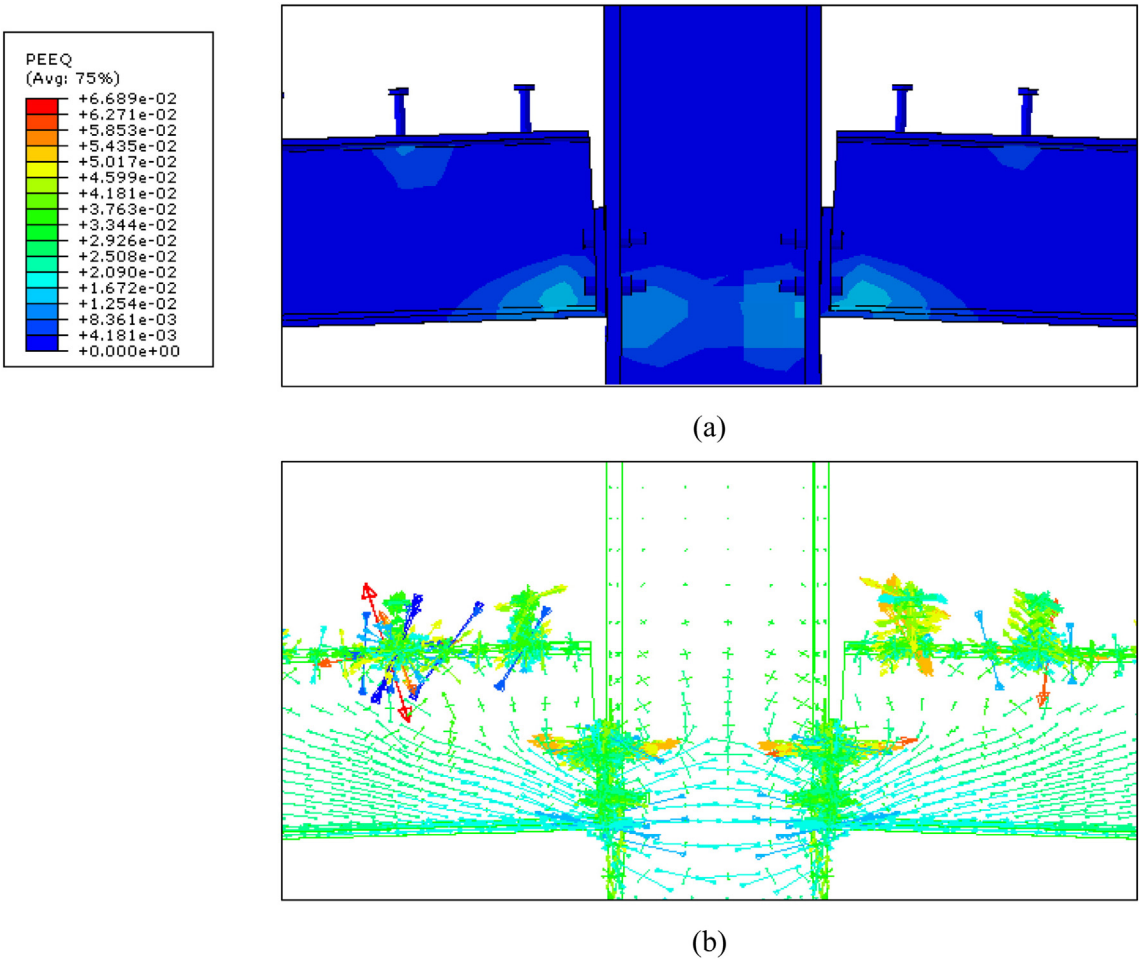

Fig. 10. FE results for the M0-iso model under the 'gravitational' loading condition (ABAQUS), with evidence of stress distribution in the steel components (6.5 mm the control point deflection, front view). (a) Plastic regions and (b) vectorial representation of principal stresses.

(with concrete slab and steel rebars hidden from view), as observed at a vertical deflection of 6.5 mm, giving evidence of the involvement of the column web on the overall resisting mechanism of the specimen.

4.3. Antisymmetric loading condition

A further loading configuration, intended to represent a distribution of internal forces in the elements which is typical of equivalent quasi-static horizontal loads, such as earthquakes or wind, was finally explored (see Fig. 5(c)). Major results for the antisymmetric loading condition, were compared for all the examined geometrical configurations, giving evidence of major FE results at the assembly as well as at the component level.

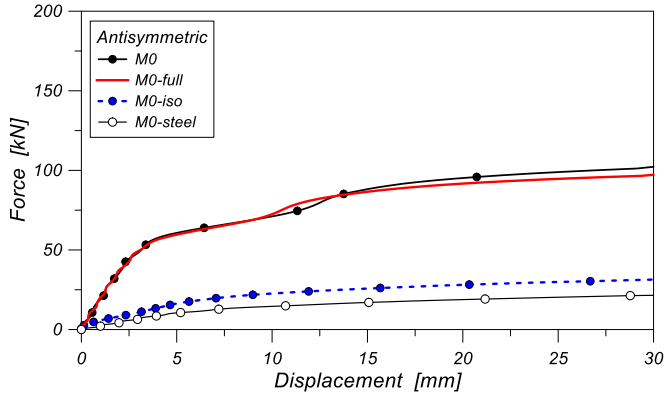

Fig. 11. FE load-displacement results, as obtained for the reference full-scale specimen and for the examined FE models under the 'antisymmetric' loading condition (ABAQUS).

As shown in Fig. 11, it is possible to notice that assuming a fully isolated concrete slab would correspond to the actual structural behaviour of the steel members only (i.e. 'M0-iso' model, with almost the same behaviour of the 'M0-steel' model). A small amount of additional resistance contribution was observed to derive, for the 'M0-iso' model compared to the 'M0-steel' solution, from continuous rebars only. Moreover, the initial stiffness of the 'M0-iso' model proved to have the same order of magnitude of the 'M0-steel' model, hence suggesting the assumption of a perfect hinge behaviour. This is not the case of the 'M0' and 'M0-full' systems, which - due to the contact at the slab-to-column interface - compared to previous 'M0-steel' and 'M0-iso' configurations offer additional stiffening and strengthening.

Figs. 12–14 present further comparative results for the same loading configuration, giving evidence of the evolution of stresses and deformations in all the specimen components. In Fig. 12, contour plots representative of the 'M0-steel' model response are provided. First yielding occurred in the joint flanges and in the beams web, at a vertical deflection of the control point in the order of 10 mm, corresponding to a vertical load $P = 4.9$ kN (see Fig. 12(a), where plastic hinges are represented). As far as the beams exhibit plastic strains, both the steel bolts and the column web are still in the elastic stage, with maximum Von Mises stresses in the range of 600 MPa and 200 MPa, respectively. Yielding of bolts manifests for higher deflections only, in the order of 12 mm, corresponding to an applied load $P = 6.8$ kN (see Fig. 12(b)). Through the simulation on the 'M0-steel' model, as also in accordance

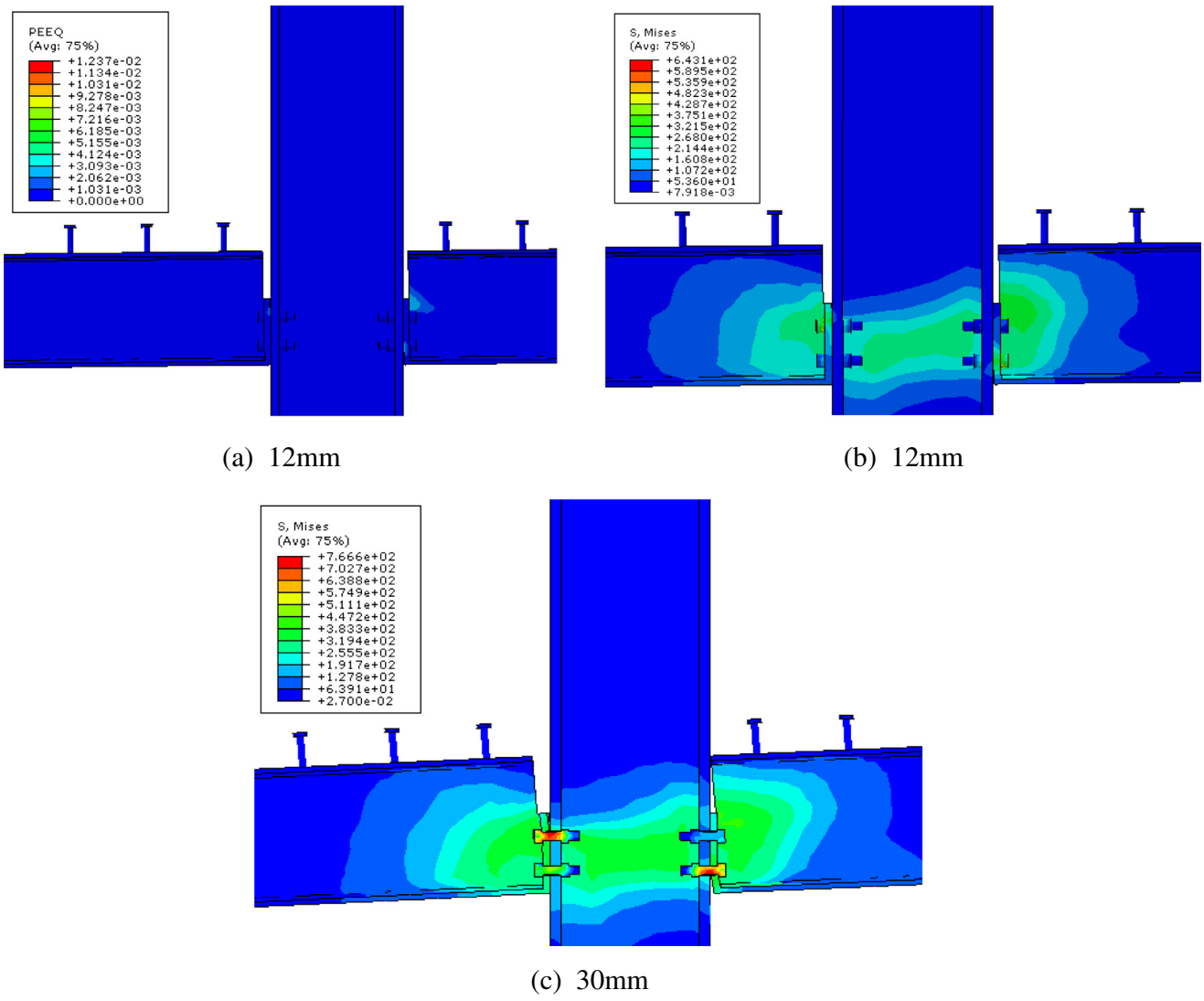

Fig. 12. FE results for the M0-steel model under the 'antisymmmetric' loading condition (ABAQUS), with evidence of (a) first yielding (plastic hinges) and (b) stress distribution in the steel components (12 mm the control point deflection); (c) stress distribution at 30 mm of deflection. Stress values given in MPa.

with Fig. 11, the contribution of bolts proved to represent the major resisting component for the full steel joint. The FE simulation was in fact stopped at a vertical deflection of the control point of 30 mm (i.e. representative of contact between the R beam and the column flange, see Fig. 12(c)), with maximum stresses in bolts in the range of 760 MPa. Given the 'M0-iso' model geometry, in accordance with Fig.

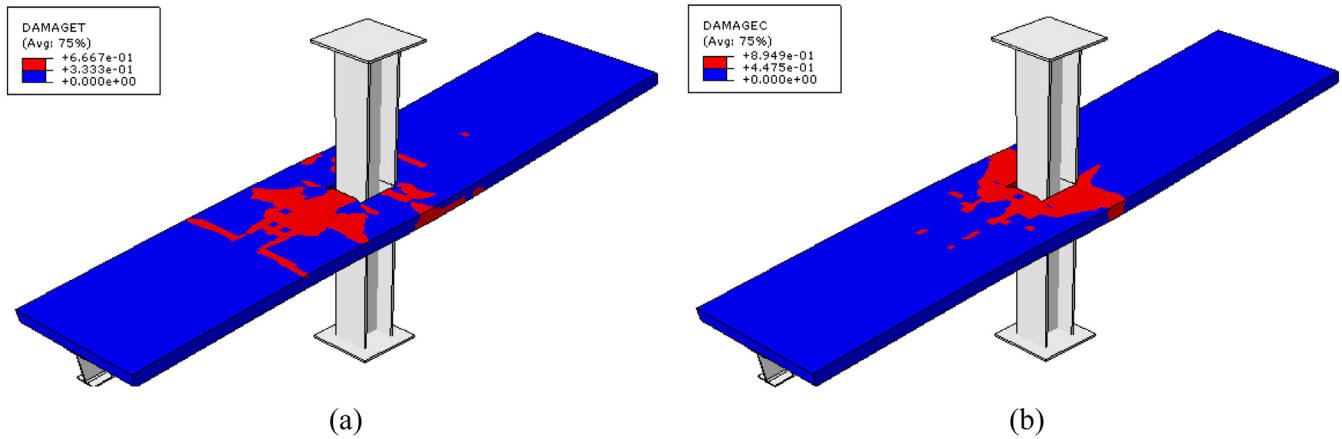

Fig. 13. FE results for the 'M0-iso' model under the 'antisymmetric' loading condition (ABAQUS), with evidence of (a) tensile damage propagation in the concrete slab (30 mm the deflection) and (b) corresponding compressive damage. Key: blue = uncracked, red = cracked. (For interpretation of the references to color in this figure legend, the reader is referred to the web version of this article.)

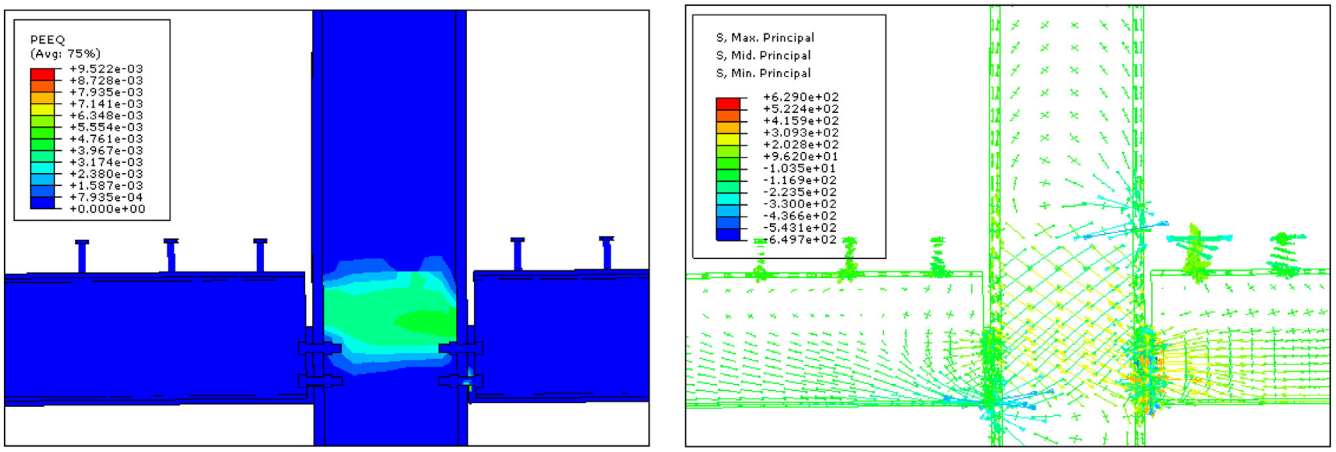

Fig. 14. FE results for the M0-full model under the antisymmetric loading condition (ABAQUS), with evidence of (a) yielding (plastic hinges) and (b) corresponding distribution of stresses in the steel components (5 mm of vertical deflection at the control point). Stress values given in MPa.

11, minor benefits were observed on the overall response of the specimen, compared to the 'M0-steel' configuration, due to lack of any mechanical interaction of the concrete slab with the steel members. Failure mechanism in the 'M0-iso' system also highlighted a rather premature propagation of cracks in the concrete slab (see for example Fig. 13).

Major effects in the observed overall behaviour of the examined joint were indeed noticed for the 'M0' and 'M0-full' configurations, due to progressive involvement of the concrete slab in the resisting mechanism of the specimen. These strut-tie mechanisms can be traced back to the 'mechanism 1' (i.e. direct compression on the column flange) and 'mechanism 2' (i.e. compressed concrete struts, inclined to the column sides), as also described in the Eurocode 8 [1]. At the design stage of steel-concrete composite joints under seismic loads, in order to apply the capacity design concept, huge effort is usually required to govern the behaviour of these mechanisms.

As also in accordance with Fig. 11, marked increase in the joint stiffness was in fact measured, compared to the steel members only as well as to the specimen with fully isolated slab. The stiffening contribution was estimated up to ≈5 times the 'M0-steel' model. No obvious variations were noticed on the overall response of the 'M0' or 'M0-full' systems, for the reference loading condition.

In terms of stress distribution and propagation in the steel components, important effects were noticed for both the 'M0' and 'M0-full' models, as compared to the previous configurations. As far as yielding first exhibits in the steel flange, in fact, the fully interacting concrete slab involves the web column in the overall resisting mechanism. As such, plastic strains are observed in the column itself (see Fig. 14(a) and (b)). In terms of damage propagation in the slab, tensile cracking and crushing mechanisms proved to have distribution in agreement with Fig. 13(a) and (b). The lack of any gap at the concrete-to-steel interface, in this sense, typically resulted in premature cracking phenomena in the slab, given the absence of possible relative adjustments before transmission of contact stresses.

5. Design considerations and resisting mechanism for the joint with fully isolated slab

A final critical analysis of the proposed FE numerical results shows, as emphasized in Section 4, that the overall behaviour of the examined joint typology under hogging moment (on both the L and R beams, as well as in the gravitational case) or antisymmetric loads is highly influenced by the contact interactions at the slab-to-column interface.

A further FE simulation - here not presented for sake of brevity - was hence carried out for completeness on the same FE models, by taking into account the presence of sagging moments (with the loaded R beam only).

Careful consideration was paid especially for the 'M0' and 'M0-iso' conditions. Basically, as also emphasized by a critical discussion of all the collected FE results, for the joint under hogging or sagging moments some important outcomes were observed. The typical resisting mechanisms manifesting in the M0 joint with fully interacting slab - and conventionally detected as strut-tie resisting mechanisms type '1' and '2' - were in fact found to agree with Eurocode 8 - Annex C provisions [1]. These mechanisms, as known, are in fact mostly related to the tensile resistance of longitudinal and transversal rebars, and typically manifest as far as any kind of interaction is provided between the slab and the column.

As far as any kind of contact interaction is avoided between the slab and the column (as in the case of the 'M0-iso' condition), in this context, it is hence intuitively expected that the same 'mechanisms 1' and '2' would not occur, with the overall structural performance of the joint being mostly affected by the resistance and stiffness of the steel members only.

This is true especially for certain loading conditions, however, as also partly emphasized in Section 4, the current FE research study highlighted that for the 'M0-iso' configuration with fully isolated slab, a further resisting mechanism (herein labelled as 'mechanism 4', in order to distinguish it from conventional Eurocode '1', '2' and '3' mechanisms type definitions) occurs.

Such 'mechanism 4' proved, for both the 'M0-iso' system under hogging or sagging moment, basically consists in the occurrence of additional struts in the slab, with 45° their slope with respect to the beam longitudinal axis, and directly propagating from the regions of contact between the slab and steel shear studs. Worth of interest - as also highlighted from full 3D simulations partly emphasized in Section 4 for hogging moments only - is that the same struts can manifest in the isolated slab both in presence of direct compressive loads in the slab (i.e. for the joint under sagging loading conditions), as well as in presence of indirect compression loads (i.e. as in the case of the composite joint under L or R hogging moment conditions), due to continuity of longitudinal rebars.

The performed FE analyses carried out on the 'M0-iso' system highlighted, in particular, that for the examined joint such struts generally propagate over a total length l equal to ≈2/3 the shear length l_v. Consequently, given n_l the number of shear studs over the reference

size l, the actual resisting contribution of the 'mechanism 4' can be rationally expected to be equal to:

$$F_{\mathrm{Rd},4} = n_l \cdot P_{Rd} \tag{12}$$

with P_{Rd} the shear resistance of a single stud, as conventionally given by Eurocode 4 provisions [2]:

$$P_{Rd} = \min\begin{cases} \dfrac{0.8\, f_u\, \pi\, d^2}{4}/\gamma_v \\ \dfrac{0.29\alpha\, d^2 \sqrt{f_{ck} E_{cm}}}{\gamma_v} \end{cases} \tag{13}$$

where $\gamma_v = 1.25$ is a partial safety coefficient, d the stud diameter, f_u its ultimate resistance and:

$$\alpha = \min\begin{cases} 1 & h_{sc}/d \geq 4 \\ 0.2 \cdot (h_{sc}/d + 1) & 3 < h_{sc}/d < 4 \end{cases} \tag{14}$$

where h_{sc} denotes the stud length.

In Fig. 15, selected FE contour plots are proposed for the 'M0-iso' model only, together with the corresponding schematic representation, to emphasize the observed behaviour for the concrete slab when subjected to sagging and hogging moments respectively (loads applied on the L beam).

5.1. Design requirements for 'mechanism 4' activation

As a key aspect for the behaviour of the concrete slab (both in compression – sagging moment – or in tension – hogging moment), see Fig. 15(a) and (b), the activation of the strut-tie 'mechanism 4' is strictly related to the amount of transversal rebar in the slab. Given the maximum resistance contribution offered by the shear studs, see Eqs. (12)–(14), the minimum amount of transversal rebar should in fact at least be equal to:

$$A_{T,4} \geq \frac{n_l P_{Rd}}{f_{yd,T}} \tag{15}$$

with n_l and P_{Rd} previously defined, while $f_{yd,T}$ denotes the design yielding stress for the transversal rebars only. The steel rebar amount $A_{T,4}$, as also in accordance with Fig. 15, is intended uniformly distributed in the slab, over a length l from the column axis.

In the case of concrete slab under tensile loads (hogging moment), where the typical mechanism occurrence is reproduced in Fig. 15(c) and (d), a crucial role in the activation of the 'mechanism 4' is played by the longitudinal rebar. There, a ductile mechanism in the joint can be privileged as far as first yielding of rebars manifests in advance to struts crushing or failure of shear studs. As such, longitudinal rebar amount should not exceed a maximum value given by:

$$A_{L,4} \leq \frac{n_l P_{Rd}}{f_{yd,L}}, \tag{16}$$

with $f_{yd,L}$ representing the design yielding stress for the longitudinal rebar, while n_l and P_{Rd} are defined by Eqs. (12)–(14).

From a theoretical point of view, such mechanism may also occur in the case of full contact between the column and the slab. It is plausible that the same mechanism has not been recognized before because mechanisms '1' and '2' - due to their higher stiffness - lead to premature crushing of the struts before the 'mechanism 4' is activated. The 'mechanism 4', in this regard, could be activated by increasing the ductility of resisting mechanisms actually proposed by the Eurocode, and for example seizing the transversal rebar to start yielding before crushing of concrete could manifest, as also suggested in [21]. In

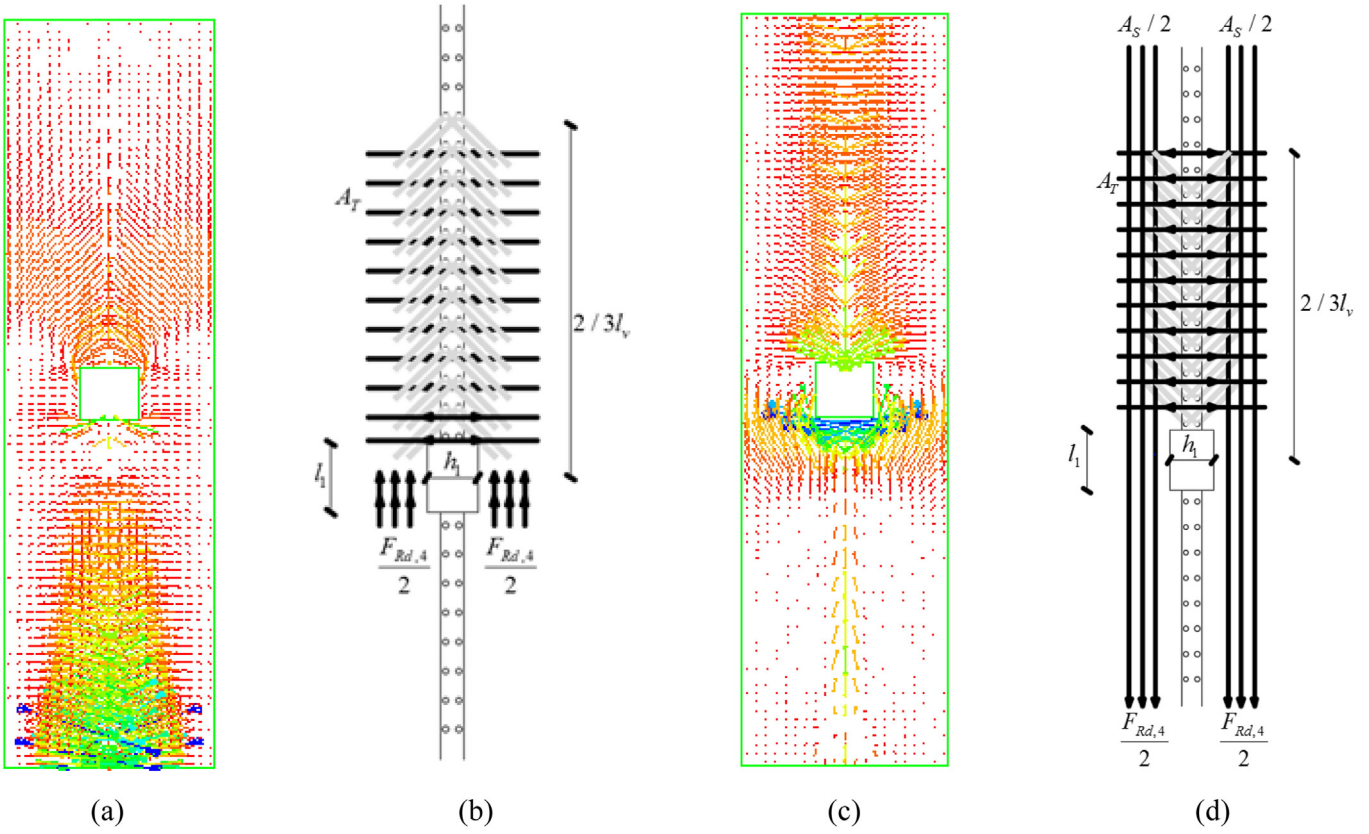

Fig. 15. Mechanism 4 for the slab under (a)–(b) sagging and (c)–(d) hogging moment, top view. FE results for the M0-iso model (vectorial representation, ABAQUS) and corresponding schematic representation.

conclusion, the actual FE exploratory investigation gave evidence of the important effects that a fully isolated slab can have on the overall response of steel-concrete composite joints under various loading configurations. Before general considerations of practical interest for design could be derived, however, additional sets of parametric analyses should be carried out, so that the current outcomes could be further assessed and validated by taking into account multiple mechanical and geometrical features for the examined joint typology. In any case, it is expected that the actual research findings here summarized could provide useful background for the optimal design of the examined joints.

6. Summary and conclusions

In the paper, a refined Finite Element (FE) numerical modelling approach derived from earlier research studies of literature was proposed to assess the actual structural response of steel-concrete composite joints under various loading conditions. In doing so, careful consideration has been paid for the evaluation and critical discussion of the effects deriving from possible slab-to-column interactions.

To this aim, a reference full-scale experimental test was derived from literature, so as to provide validation of FE assumptions and calibrations, as well as to allow further extension of the same investigation.

Careful attention was paid, in particular, for four total geometrical configurations for the reference semi-rigid steel-concrete composite joint, being characterized by (i) absence of slab, (ii) presence of slab with partial interaction with the column (i.e. isolated slab) and (iii) presence of almost fully interacting slab (i.e. even with a small gap on one side only), giving evidence of corresponding effects.

It was shown, in particular, that the actual slab isolation leads to important effects on the structural performance of the full composite joint, hence requiring specific design considerations.

As far as current outcomes are considered within the set of design recommendations in use for steel-concrete composite joints, the overall performance of a joint with isolated slab and continuity of longitudinal rebar in braced systems proved in fact to ensure:

a) a bending resistance moment, under gravitational loads, comparable with those of a fully interacting composite joint;
b) stiffness and resistance performances almost identical to those of a hinged joint, under antisymmetric loads, being representative of equivalent quasi-static horizontal loads deriving from seismic events or wind pressures.

As such, major implicit advantages for design purposes are that:

a) under gravitational loads, the beam can be considered as continuous on multiple supports. A reduction of sagging moment at mid-span is thus expected on the composite beam section;
b) under horizontal loads, the complex interaction between the concrete slab and the column is avoided, hence allowing a marked simplification of the full design process.

Acknowledgments

DPC-RELUIS is gratefully acknowledged for funding the research activity within the framework of “Steel and steel-concrete composite structures” project (2015–2018).

References

[1] Eurocode 8, Design Provisions for Earthquake Resistance of Structures. Part 1.3: General Rules. Specific Rules for Various Materials and Elements, CEN, European Committee for Standardisation, Brussels, Belgium, 2004.
[2] Eurocode 4, Design of Composite Steel and Composite Structures. Part 1.1: General Rules and Rules for Buildings, CEN, European Committee for Standardisation, Brussels, Belgium, 2008.
[3] J. Aribert, A. Ciutina, D. Dubina, Seismic response of composite structures including actual behaviour of beam-to-column joints, Composite Construction in Steel and Concrete V 2006, pp. 708–717, https://doi.org/10.1061/40826(186)66.
[4] R. Zandonini, Semi-rigid composite joints, in: Narayanan (Ed.), Structural Connections Stability and Strength, Chapter 3, Elsevier Applied Science, London (UK) 1989, pp. 63–120.
[5] S.-J. Lee, L.-W. Lu, Cyclic tests of full-scale composite joint subassemblages, J. Struct. Eng. 115 (8) (1989) 1977–1998.
[6] J.Y.R. Liew, T.H. Teo, N.E. Shanmugam, C.H. Yu, Testing of steel–concrete composite connections and appraisal of results, J. Constr. Steel Res. 56 (2000) 117–150.
[7] O.S. Bursi, G. Gramola, Behaviour of composite substructures with full and partial shear connection under quasi-static cyclic and pseudo-dynamic displacements, Mater. Struct. 33 (2000) 154–163.
[8] R. Simões, L. Simões da Silva, P. Cruz, Experimental behaviour of end-plate beam-to-column composite joints under monotonical loading, Eng. Struct. 23 (2001) 1383–1409.
[9] R. Simões, L. Simões da Silva, Cyclic behaviour of end-plate beam-to-column composite joints, Steel Compos. Struct. 1 (3) (2001) 355–376.
[10] T.P. Green, R.T. Leon, G.A. Rassati, Bidirectional tests on partially restrained, composite beam-to-column connections, J. Struct. Eng. 130 (2) (2004) 320–327 (Special Issue: Composite and Hybrid Structures).
[11] J.Y.R. Liew, T.H. Teo, N.E. Shanmugam, Composite joints subject to reversal of loading—part 1: experimental study, J. Constr. Steel Res. 60 (2004) 221–246.
[12] J.Y.R. Liew, T.H. Teo, N.E. Shanmugam, Composite joints subject to reversal of loading—part 2: analytical assessment, J. Constr. Steel Res. 60 (2004) 247–268.
[13] M. Nakashima, T. Matsumiya, K. Suita, F. Zhou, Full-scale test of composite frame under large cyclic loading, J. Struct. Eng. 133 (2) (2007) 297–304.
[14] A. Braconi, O.S. Bursi, G. Fabbrocino, W. Salvatore, R. Tremblay, Seismic performance of a 3D full-scale high-ductility steel–concrete composite moment-resisting structure—part I: design and testing procedure, Earthq. Eng. Struct. Dyn. 37 (2008) 1609–1634.
[15] G. Vasdravellis, M. Valente, C.A. Castiglioni, Behavior of exterior partial-strength composite beam-to-column connections: experimental study and numerical simulations, J. Constr. Steel Res. 65 (2009) 23–35.
[16] F.M. Mazzolani, Mathematical model for semi-rigid joints under cyclic loads, in: R. Bjorhovde, et al., (Eds.), Connections in Steel Structures: Behaviour, Strength and Design, Elsevier Applied Science Publishers, London 1988, pp. 112–120.
[17] W. Salvatore, O.S. Bursi, D. Lucchesi, Design, testing and analysis of high ductile partial-strength steel–concrete composite beam-to-column joints, Comput. Struct. 83 (28–30) (2005) 2334–2352.
[18] F. Zhou, K.M. Mosalam, M. Nakashima, Finite-element analysis of a composite frame under large lateral cyclic loading, J. Struct. Eng. 133 (7) (2007) 1018–1026.
[19] A. Braconi, W. Salvatore, R. Tremblay, O.S. Bursi, Behaviour and modelling of partial-strength beam-to-column composite joints for seismic applications, Earthq. Eng. Struct. Dyn. 36 (2007) 142–161.
[20] A. Braconi, O.S. Bursi, G. Fabbrocino, W. Salvatore, F. Taucer, R. Tremblay, Seismic performance of a 3D full-scale high-ductility steel–concrete composite moment-resisting structure— part II: test results and analytical validation, Earthq. Eng. Struct. Dyn. 37 (2008) 1635–1655.
[21] C. Amadio, C. Bedon, M. Fasan, M.R. Pecce, Refined numerical modelling for the structural assessment of steel-concrete composite beam-to-column joints under seismic loads, Eng. Struct. 138 (2017) 394–409.
[22] Simulia, ABAQUS Computer Software V.6.12. Theory Manual, Dassault Systems, 2012.
[23] R. Puhali, I. Smotlak, R. Zandonini, Semi-rigid composite action: experimental analysis and a suitable model, J. Constr. Steel Res. 15 (1–2) (1990) 121–151.
[24] X. Liu, M.A. Bradford, Q.-J. Chen, H. Ban, Finite element modelling of steel-concrete composite beams with high-strength friction-grip bolt shear connectors, Finite Elem. Anal. Des. 108 (2016) 54–65.
[25] A. Prakash, N. Anandavalli, C.K. Madheswaran, J. Rajasankar, N. Lakshmanan, Three dimensional FE model of stud connected steel-concrete composite girders subjected to monotonic loading, Int. J. Mech. Appl. 1 (1) (2011) 1–11.
[26] J. Zeng, P. Mäkeläinen, Finite element modelling of semi-rigid composite joints in a slim floor frameProceedings of Nordic Steel Construction Conference - NSCC 2009, Malmö, Sweden, 2–4 September 2009, pp. 335–342 (ISBN 91-7127-058-2).
[27] Z. Wang, J. Pan, J. Yuan, The study on semi-rigid joint of steel-concrete composite beam to CFST column, Adv. Steel Constr. 5 (4) (2009) 421–431.
[28] D. Lam, Recent research and development in semi-rigid composite joints with precast hollowcore slabs, Proceedings of the Sixth International Workshop on Connections in Steel Structures, 23–25 June, Chicago, USA, 2008.
[29] D. Lam, X. Dai, T. Sheehan, An experimental study on flexural and shear behaviour of intermediate-to-long spanning composite beams, DISSCO Report - Development of Improved Shear Connection Rules in Composite Beams, 2015.
[30] J. Qureshi, D. Lam, J. Ye, Effect of shear connector spacing and layout on the shear connector capacity in composite beams, J. Constr. Steel Res. 67 (2011) 706–719.
[31] T. Jankowiak, T. Lodygowski, Identification of Parameters of Concrete Damage Plasticity Constitutive Model. Foundation of Civil and Environmental Engineering, 6, Poznan university of technology, Poland, 2005 53–69.
[32] EN 1992-1-1, Eurocode 2: Design of Concrete Structures: Part 1–1: General Rules and Rules for Buildings, CEN, Brussels, Belgium, 2004.
[33] Y. Huang, Z. Yang, W. Ren, G. Liu, C. Zhang, 3D meso-scale fracture modelling and validation of concrete based on in-situ X-ray computed tomography images using damage plasticity model, Int. J. Solids Struct. 67-68 (2015) 340–352.
[34] O. Martin, Comparison of Different Constitutive Models for Concrete in ABAQUS/Explicit for Missile Impact Analyses. European Commission - Joint Research Centre - Institute for Energy, 2010https://doi.org/10.2790/19764 http://europa.eu/(Report JRC 56256, EUR 24151 EN).

[35] Y. Dere, M.A. Koroglu, Nonlinear FE modeling of reinforced concrete, Int. J. Struct. Civil Eng. Res. 6 (1) (2017) 71–74, https://doi.org/10.18178/ijscer.6.1.71-74.
[36] A.S. Genikomsou, M.A. Polak, in: Saouma, Bolander, Landis (Eds.),Damaged plasticity modelling of concrete in finite element analysis of reinforced concrete slabsProceedings of 9th International Conference on Fracture Mechanics of Concrete and Concrete Structures - FraMCoS-9, 2016https://doi.org/10.21012/FC9.006.
[37] P. Kmiecik, M. Kaminski, Modelling of reinforced concrete structures and composite structures with concrete strength degradation taken into consideration, Arch. Civ. Mech. Eng. XI (3) (2011) 623–636.
[38] Z. Huang, Y. Tu, Modelling of damage and its use in assessment of prestressed concrete bridge, Proceedings of 19th IABSE Congress - Challenges in Design and Construction of an Innovative and Sustainable Built Environment, Stockholm, 21–23 September2016.
[39] C. Bedon, M. Fragiacomo, Three-dimensional modelling of notched connections for timber-concrete composite beams, Struct. Eng. Int. (2) (2017) 184–187, https://doi.org/10.2749/101686617X14881932435295.
[40] N. Gattesco, C. Amadio, C. Bedon, Experimental and numerical study on the shear behaviour of stone masonry walls strengthened with GFRP reinforced mortar coating and steel-cord reinforced repointing, Eng. Struct. 5 (2015) 143–147.
[41] C. Bedon, C. Louter, Finite-element analysis of post-tensioned SG-laminated glass beams with mechanically anchored tendons, Glass Struct. Eng. 1 (1) (2016) 19–37, https://doi.org/10.1007/s40940-0167.
[42] V. Birtel, P. Mark, Parameterised finite element modelling of RC beam shear failureProceedings of 2006 ABAQUS Users' Conference 2006, pp. 95–108.
[43] H.A.W. Cornelissen, D.A. Hordijk, H.W. Reinhardt, Experimental determination of crack softening characteristics of normal weight and lightweight concrete, Heron 31 (2) (1986) 45–56.
[44] Z.P. Bažant, Concrete fracture models: testing and practice, Eng. Fract. Mech. 69 (2002) 165–205.
[45] M. D'Aniello, R. Tartaglia, S. Costanzo, R. Landolfo, Seismic design of extended stiffened end-plate joints in the framework of Eurocodes, J. Constr. Steel Res. 128 (2017) 512–527.